We are IntechOpen, the world's leading publisher of Open Access books Built by scientists, for scientists

6,900
Open access books available

185,000
International authors and editors

200M
Downloads

154
Countries delivered to

Our authors are among the

TOP 1%
most cited scientists

12.2%
Contributors from top 500 universities

BOOK CITATION INDEX
CLARIVATE ANALYTICS
INDEXED

WEB OF SCIENCE™

Selection of our books indexed in the Book Citation Index
in Web of Science™ Core Collection (BKCI)

Interested in publishing with us?
Contact book.department@intechopen.com

Intercalation of Poly[Oligo(Ethylene Glycol) Oxalate] into Vanadium Pentoxide Xerogel: Preparation, Characterization and Conductivity Properties

Evans A. Monyoncho, Rabin Bissessur,
Douglas C. Dahn and Victoria Trenton

Additional information is available at the end of the chapter

Abstract

We report, for the first time, the intercalation of poly[oligo(ethylene glycol) oxalate] (POEGO) and POEGO lithium salt ($LiCF_3SO_3$) complex (POEGO-$LiCF_3SO_3$) into vanadium pentoxide xerogel ($V_2O_5nH_2O$). The effect of changing the polymer concentration on the interlayer expansion of the layered host was studied, and the optimal intercalation ratio was determined to be 1:2. The intercalates were characterized by powder X-ray diffraction, thermogravimetric analysis, differential scanning calorimetry, Fourier transform infrared spectroscopy, and AC impedance spectroscopy.

Keywords: Layered structures, Nanocomposites, Electrical properties, Infrared (IR) spectroscopy, X-ray diffraction

1. Introduction

Intercalation chemistry is a versatile technique for developing new materials at moderate conditions. Unlike other techniques such as organic syntheses where rigorous conditions are used and purification of products is mandatory, intercalation chemistry provides an excellent route to combine the properties of two materials, which often does not require product purification. Therefore, intercalation chemistry is a "green shift" for developing new materials. Vanadium pentoxide xerogel ($V_2O_5nH_2O$) is a layered structure of interest to researchers in both academia and industry. This is because $V_2O_5nH_2O$ nanocomposites have potential applications such as in electrochemical energy storage devices [1, 2], biosensors [3], and

electrochromic devices [4]. Most of the research on $V_2O_5 nH_2O$ xerogel nanocomposites is focused in developing energy storage materials to address the current demands for renewable and portable electrical energy.

Intercalation of polymers into layered structures is a growing field of research with a wide range of potential applications [5]. For example, organic–inorganic nanocomposites offer promise for new engineering composites in the automotive, packaging, and aerospace industry because of their improved mechanical properties [6]. An organic–inorganic nanocomposite is a two-phase material in which the organic and inorganic phases are distributed in each other at the nanolevel. Therefore, with careful selection of the inorganic host and the guest polymer, it is possible to design materials that can be used in electrochemical energy storage devices such as in Li-ion batteries. Normally, the nanocomposite composition is controlled in order to increase its ionic conductivity at ambient temperatures so that it can be used as a solid electrolyte and/or as a cathode.

Vanadium pentoxide xerogel is a good host material for guest molecules and ions. The intercalation of guest species into vanadium pentoxide xerogel may occur via dipole–dipole interaction, ion exchange, acid–base, coordination, and redox reactions, enabling the system to accept both neutral and charged guest species [7, 8]. Vanadium pentoxide xerogel has also shown promising redox reactions that can be utilized in Li-ion batteries. For example, Passerini et al. demonstrated that $V_2O_5 nH_2O$ xerogel could be used as a cathode material that reversibly intercalates more than three equivalents of lithium [9].

Current conventional Li-ion batteries utilize liquid organic electrolytes [10, 11] that come with several shortcomings, which limit their widespread usage in large load applications, such as electric vehicles and stationary power. Most of these liabilities are safety-related, which include electrolyte leakage, decomposition, flammability, and a propensity to develop catastrophic short circuits. To circumvent these problems, polymer electrolytes have been extensively studied as an alternative. The search for polymer electrolytes was initiated by the discovery of ionic conduction in complexes of poly(ethylene oxide) (PEO) containing alkali metal salts [12, 13] and the suggestion that such ionic conductors could be used as electrolytes in electrochemical devices [14]. Since then many PEO derivatives have been developed with efforts to improve ionic conductivity [15, 16]. There are two main strategies used for developing PEO derivatives with increased ionic conductivity: one approach focuses on increasing ionic mobility, that is, developing polymers that are flexible and amorphous with low glass transition temperatures. The second strategy focuses on increasing ionic dissociation by placing polar subunits such as acrylamide, acrylonitrile, maleic anhydride, and carbonate along the chains to increase the polymer's dielectric constant [17, 18]. Based on the second strategy, poly[oligo(ethylene glycol)-oxalate] (POEGO) was developed by Xu et al. [19]. They reported a maximum conductivity of 5.9×10^{-5} S cm^{-1} at 25°C with the complex of lithium bis(trifluoromethanesulfonyl)imide (LiTFSI), with etheric oxygen to Li-ion ratio of [EO]/[Li$^+$] = 16. They also reported that POEGO–LiTFSI complex showed good electrochemical stability up to 4.4 V versus Li$^+$/Li. These properties make POEGO a viable candidate for developing solid electrolytes for Li-ion batteries.

Several studies have been conducted where POEGO is intercalated into various layered structures. The intercalation is meant to improve the mechanical properties of POEGO in order to eliminate its tendency to flow under pressure, while retaining its ionic conductivity, and hence make it more suitable for use as a solid electrolyte in Li-ion batteries. For example, POEGO has been intercalated into hectorite [20], tin disulfide [21], graphite oxide [22], and molybdenum disulfide [23]. To our best knowledge, no work has been reported on the intercalation of POEGO into $V_2O_5 n H_2O$ xerogel.

The focus of this chapter is to report on the intercalation of POEGO and $LiCF_3SO_3$–POEGO complex into vanadium pentoxide xerogel and the potentials of these nanocomposites in the Li-ion battery applications. In this chapter, the lithium salt ($LiCF_3SO_3$) and a complex of POEGO with $LiCF_3SO_3$ will be abbreviated as LiX ($X = CF_3SO_3$) and Li-POEGO, respectively. The nanocomposites will be abbreviated as V_2O_5POEGO and V_2O_5Li-POEGO followed by the mole ratio (e.g., V_2O_5POEGO 1:1).

2. Experimental

2.1. Materials

Sodium metavanadate was purchased from Fluka. Dowex 50W-X 8, 20–50 mesh resin, and oxalic acid dihydrate were purchased from Baker. HPLC-grade methanol was purchased from Caledon. Benzene 99.9% was purchased from Aldrich. All were used as received. Poly(ethylene glycol) (PEG 400), purchased from Aldrich was dried over 3 Å molecular sieves under nitrogen purge from a Schlenk line.

2.2. Vanadium pentoxide xerogel ($V_2O_5 n H_2O$) synthesis

The synthesis of $V_2O_5 n H_2O$ was adapted from the literature [24]. In this work, sodium metavanadate (4.0 g, 0.033 mol) was dissolved in deionized water (150 mL). The resulting colorless solution was then passed through an acidic ion exchange column (510 mEq capacity) made from Dowex 50W-X8, 20–50 mesh resin. The collected eluate (200 mL) was the yellow-brownish polyvanadic acid (HVO_3). The excess water was evaporated from the HVO_3 at room temperature for 2 weeks, and the solution was polymerized into a dark-red xerogel ($V_2O_5 n H_2O$) solution. The $V_2O_5 n H_2O$ solution was used without further dilution in the subsequent intercalation reactions.

2.3. Synthesis of poly[oligo(ethylene glycol) oxalate] (POEGO)

POEGO was synthesized as reported in the literature [19]. In a typical experiment, PEG 400 (15.0 g, 0.0375 mol) was added to oxalic acid dihydrate (5.00 g, 0.0397 mol) in benzene (100 mL), and the mixture was refluxed for 4 days in a 250 mL round-bottom flask while stirring. Benzene was then removed under reduced pressure. The reaction mixture was then heated in a vacuum oven at 120°C until a clear viscous product was obtained. The use of PEG with a

molecular weight of 400 means that there are, on average, nine ethyleneoxy repeating units in each oligo(ethylene glycol) oxalate group in our POEGO [19].

A Li-POEGO complex was prepared using the optimum ionic conductivity ratio of $[EO]/Li^+ = 16$ as reported in the literature [19].

2.4. Synthesis of nanocomposites

The nanocomposites were prepared by adding POEGO dissolved in methanol to the aqueous solution of $V_2O_5nH_2O$, with stirring at room temperature in air for 30 min. In a typical experiment of mole ratio 1:1, 13.0 mL of the xerogel (0.160 g, 7.40×10^{-4} mol) was mixed with 1.0 mL of POEGO solution in methanol (1.25×10^{-4} mol). The following mole ratios were prepared: 1:0.5, 1:1, 1:2, 1:3, and 1:4. The mole ratios were calculated based on moles of $V_2O_51 \bullet 9H_2O$ and moles of POEGO's repeat unit. From here on, the nanocomposites will be referred to as V_2O_5POEGO followed by the mole ratio (e.g., V_2O_5POEGO 1:1 for the mole ratio of 1 to 1).

To confirm that the polymer chains were actually intercalated into $V_2O_5nH_2O$ and not just the solvent, a control sample was prepared and characterized. The control sample was prepared by adding 5.0 mL of methanol (the solvent used for dissolving POEGO) into 10.0 mL of an aqueous solution of $V_2O_5nH_2O$ gel, and stirring the mixture for 30 min. From here on, this control sample will be denoted as V_2O_5MeOH.

2.5. Materials characterization

Powder X-ray diffraction (XRD) data were collected on a Bruker AXS D8 Advance instrument equipped with a graphite monochromator, variable divergence slit, variable antiscatter slit, and a scintillation detector. Cu (Kα) radiation ($\lambda = 1.5406$ Å) was used. Samples were prepared as dry thin films on glass substrates by casting the homogeneous solutions at room temperature in air.

Thermal properties of the samples were investigated using TA instruments. Thermogravimetric analysis (TGA) data were collected on a Q500 in dry air or nitrogen purge using a heating rate of 10°C/min up to 680°C. Differential scanning calorimetry (DSC) was performed on a Q100 under dry nitrogen purge using heating and cooling rates of 10°C/min and 5°C/min, respectively. The TGA and DSC data were processed using the TA Universal Analysis 2000 software. The samples were freeze-dried using a Virtis Benchtop 3.3/Vacu-Freeze dryer and left in a desiccator overnight, before analysis.

Reflectance Fourier transform infrared (FTIR-ATR) spectra were obtained in the range 4000–400 cm^{-1} on a Bruker ALPHA FT-IR spectrometer equipped with attenuated total reflectance (ATR) sampling unit. The resolution of the instrument was 0.9 cm^{-1}, and 128 scans were used.

Conductivity data were collected by using AC impedance spectroscopy. A Solartron 1250 frequency response analyzer, along with a home-built current-preamplifier circuit was utilized. The amplitude of the sine wave perturbation was 50 mV, and a frequency range from 10 kHz to 0.01 Hz was used. The samples were run as cast films on rectangular glass substrates. Silver paste was placed on the two ends of the films as electrodes, so that current flow was

along the film, parallel to the substrate. Prior to the conductivity measurements, samples were held in vacuum for at least 20 h at room temperature to remove any moisture and adsorbed volatile materials. During conductivity measurements, the samples remained in vacuum and were in thermal contact with an electrically heated copper sample holder cooled by a Cryodyne 350 refrigerator. A Lakeshore Cryotronics Model 321 temperature controller was used for temperature regulation. After the conductivity measurements, the glass substrates were cleaved so that the film thickness could be measured with an optical microscope.

3. Results and discussion

3.1. X-ray diffraction (XRD)

Powder XRD patterns were used to confirm the successful intercalation of POEGO and Li-POEGO into $V_2O_5nH_2O$ and the identity of the as-synthesized $V_2O_5nH_2O$. **Figure 1** shows the representative diffraction patterns for $V_2O_5nH_2O$, V_2O_5MeOH, and V_2O_5POEGO 1:1. The diffraction patterns of other nanocomposites showed similar features, and their interlayer expansions are summarized in **Table 1**. The interlayer spacing (d) for the synthesized $V_2O_5nH_2O$ was found to be 11.9 Å, and "n" was determined from TGA to be ≈1.9, which corroborates well with the literature values of d = 11.5 Å, n = 1.8 [25]. The d-spacing is dependent on the amount of intercalated water molecules. The diffraction pattern for V_2O_5POEGO 1:1 (**Figure 1**, curve c) showed a d-spacing of 20.4 Å, which corresponds to an interlayer expansion of 8.5 Å with respect to $V_2O_51.9H_2O$.
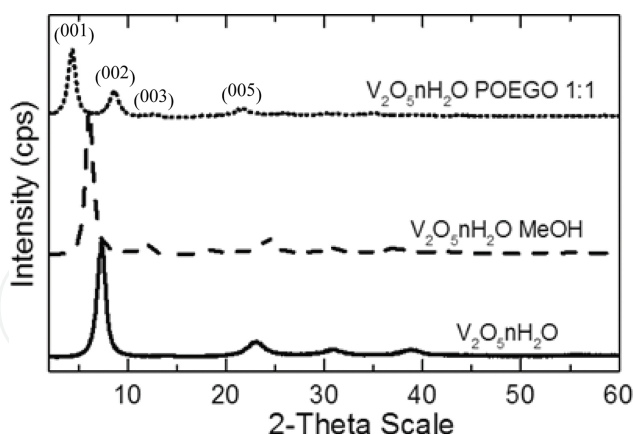

Figure 1. XRD of (a) $V_2O_5nH_2O$, (b) V_2O_5MeOH, and (c) V_2O_5POEGO 1:1.

Materials (ratios)	Observed d-spacing (Å)	Expansion Δd-spacing (Å)	Average crystallite size (Å)
$V_2O_51.9H_2O$	11.9	–	73
V_2O_5MeOH	14.5	2.6	89

Materials (ratios)	Observed d-spacing (Å)	Expansion Δd-spacing (Å)	Average crystallite size (Å)
V$_2$O$_5$POEGO (1:0.5)	17.9	6.0	79
V$_2$O$_5$POEGO (1:1)	20.4	8.5	96
V$_2$O$_5$POEGO (1:2)	20.8	8.9	85
V$_2$O$_5$POEGO (1:3)	20.6	8.7	97
V$_2$O$_5$POEGO (1:4)	21.0	9.1	70

Table 1. List of interlayer expansions and average crystallite size of the nanocomposites.

The XRD patterns of the nanocomposites showed complete intercalation of POEGO in the gallery space of the host, based on the absence of the pristine V$_2$O$_5$nH$_2$O phase. Further evidence of POEGO intercalation into V$_2$O$_5$nH$_2$O is obtained through comparison of the XRD patterns to the control sample (V$_2$O$_5$MeOH), which showed a d-space increase of 2.6 Å compared to 8.5 Å for V$_2$O$_5$POEGO 1:1. These observations are strong evidence that POEGO was actually intercalated into V$_2$O$_5$nH$_2$O. However, it is difficult to say whether methanol is co-intercalated with POEGO from the XRD pattern alone. The XRD patterns of the nanocomposites show only (00l) reflections, which is indicative of highly oriented materials.

Table 1 shows that there is no significant increase in d-spacing as the amount of POEGO increases. This observation means that the average interlayer expansion of 8.7 Å corresponds to the optimum loading of POEGO chains into V$_2$O$_5$nH$_2$O. This finding corroborates with a previous work where POEGO has been intercalated into other layered structures. For example, intercalation of POEGO into tin disulfide [21] and molybdenum disulfide [23] were reported with interlayer expansions of 8.7 and 8.6 Å, respectively. From these literature reports, the interlayer expansion was ascribed to a bilayer arrangement of POEGO chains sandwiched between the layers of the host. Using similar arguments, the average interlayer expansion of 8.7 Å in this work corresponds to a bilayer conformation of POEGO chains between the V$_2$O$_5$ ribbons.

From the XRD patterns, the average crystallite size of the nanomaterials was calculated by using the Scherrer equation.[1] As shown in Table 1, there is no clear trend of the crystallite size with the amount of POEGO present in the nanocomposite. For example, the nanocomposite with mole ratio 1:3 shows the highest crystallite size, while that with mole ratio 1:4 shows the least value.

All the nanocomposite mole ratios prepared formed homogeneous solutions that were cast into thin films for XRD and conductivity studies. However, upon freeze-drying, the solutions from mole ratios 1:3 and 1:4 separated into two solid phases. One phase was a fine powder

---

[1] The Scherrer equation is $D_{hkl} = \frac{K\lambda 57.3}{\beta cos\theta}$, where D_{hkl} = average crystallite size (Å), λ is the wavelength of the Cu (K$_\alpha$) radiation used (λ = 1.5406 Å), β = peak width at half height (2θ), and θ = position of the peak in degrees. The constant 57.3 is the conversion factor from radians to degrees. K is a constant that depends on the shape of the crystallites. The shape of our crystallites is not known. However, we use K = 0.9 (for spheres) for all samples, since we are primarily concerned with the trends, rather than the actual values.

and the other phase was a sticky mass. The two phases were characterized separately with the other techniques (TGA, DSC, and FTIR).

3.2. Thermogravimetric analysis (TGA)

The thermostability and stoichiometric composition of the nanocomposites were determined using TGA data. **Figure 2** shows the decomposition profile for POEGO, V_2O_5MeOH, V_2O_5POEGO 1:1, and V_2O_5POEGO 1:4 (the fine powder and the sticky mass). The thermograms were obtained in air using a heating rate of 10°C min^{-1}. POEGO decomposed completely in air, as shown in **Figure 2**, curve a. The control sample (V_2O_5MeOH) has the highest residue percentage of 89% as shown in **Figure 2**, curve e. Curves b and c of **Figure 2** show the decomposition profiles for V_2O_5POEGO 1:4 (sticky mass) and V_2O_5POEGO 1:4 (fine powder), respectively, while that of V_2O_5POEGO 1:1 is depicted by curve d. A complete analysis of the TGA data is summarized in **Table 2**. The nanocomposites have a weight residue percentage that corresponds to the amount of $V_2O_5nH_2O$ present.
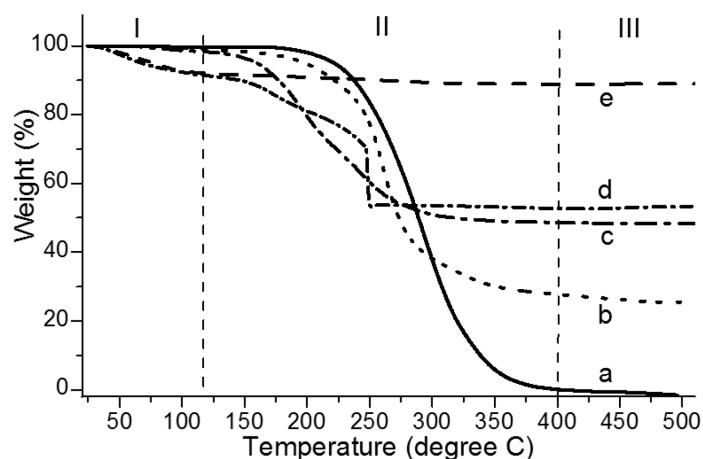

Figure 2. TGA of (a) POEGO, (b) V_2O_5POEGO 1:4 sticky mass (c) V_2O_5POEGO 1:4 powder, (d) V_2O_5POEGO 1:1, and (e) V_2O_5MeOH.

Material		Decomposition in air		Residue (wt.%)
Mole ratios used	Composition ratios	Weight (%)	Temperature (°C)^2	
POEGO		100	291	0
$V_2O_5nH_2O$	$V_2O_5(H_2O)_{1.9}$	10.3, 2.5	49; (321, 364)	84.3
V_2O_5MeOH	$V_2O_5(MeOH)_{0.7}$	8.4	80	88.8
V_2O_5POEGO (1:0.5)	$V_2O_5(POEGO)_{0.1}(H_2O)_{0.8}$	22.3	285	72.2
V_2O_5POEGO (1:1)	$V_2O_5(POEGO)_{0.3}(H_2O)_{1.8}$	36.8	248	53.5
V_2O_5POEGO (1:2)	$V_2O_5(POEGO)_{0.6}(H_2O)_1$	55.7	204	40.2
V_2O_5POEGO (1:3) f	$V_2O_5(POEGO)_{0.6}(H_2O)_{0.7}$	59.0	(205, 254)	38.1

Material		Decomposition in air		Residue (wt.%)
Mole ratios used	Composition ratios	Weight (%)	Temperature (°C)[2]	
V_2O_5POEGO (1:3) s	$V_2O_5(POEGO)_{1.1}(H_2O)_{3.2}$	68.2	209	24.1
V_2O_5POEGO (1:4) f	$V_2O_5(POEGO)_{0.4}(H_2O)_{0.3}$	49.6	(195, 245)	48.6
V_2O_5POEGO (1:4) s	$V_2O_5(POEGO)_{1.2}(H_2O)_{0.6}$	72.9	260	25.5

Note. "f" denotes the fine powder phase and "s" denotes the sticky mass phase.

Table 2. TGA data for POEGO, $V_2O_5nH_2O$, V_2O_5MeOH, and the nanocomposites.

The thermogram of the control sample (**Figure 2**, curve e) shows a constant weight residue above 100°C, that is, after the evaporation of methanol. Therefore, the weight loss process above 100°C for the nanocomposites is associated with the polymer decomposition (see **Figure 2**). Increasing the amount of POEGO in the nanocomposites decreases the residue percentage, due to the decreased concentration of $V_2O_5nH_2O$, as shown in Table 2.

For the nanocomposites which separated into two phases, the fine powder phases (**Figure 2**, curve c) yielded higher residue percentages compared to the corresponding sticky mass phases (**Figure 2**, curve b). These data mean that the sticky phases have higher polymer component than the fine powder. Interestingly, the residue percentages of the sticky phases have similar weight percentages of 24.1% and 25.5% for V_2O_5POEGO 1:3 and V_2O_5POEGO 1:4, respectively. On the other hand, the corresponding residue percentages of the fine powders are significantly different, having a difference of more than 10%. This observation means that during the phase separation, the composition of the sticky phase is independent of the amount of $V_2O_5nH_2O$ or POEGO used.

The decomposition profiles can be divided into three stages as shown in **Figure 2**. In stage I (<120°C), the weight loss corresponds to the evaporation of water/solvent. The weight loss in stage I varies randomly with no correlation to the amount of polymer used. In stage II (120–400°C), the weight loss corresponds to the decomposition of the polymer. At this stage, the percentage weight loss is directly proportional to the amount of the polymer present in the nanocomposite. Finally, stage III (>400°C) corresponds to the residue which has a constant weight percentage. The residue, yellow in color, was identified with XRD to be orthorhombic V_2O_5 crystals.

The stoichiometric compositions were calculated based on the mass loss at each of the first two stages, the mass of the residue, and the corresponding molecular weight of the compound.[3] A complete list of calculated compositions for all nanocomposites is provided in Table 2. There is no clear correlation (from Table 2) between the experimental mole ratios and the calculated

---

[2] The temperature values were taken from the peak maximum of the derivative plot. Where the derivative peaks were not well resolved (due to overlapping weight loss steps), the temperature values of the peaks are enclosed in brackets.

[3] The mass loss at stage I, stage II, and the mass of the residue (stage III) were assumed to correspond to water, POEGO, and V_2O_5, respectively. The moles of water, POEGO, and V_2O_5 were calculated for each sample. The mole ratios were expressed with respect to the moles of V_2O_5 (e.g., the composition for V_2O_5POEGO 1:1 was determined to be $V_2O_5(POEGO)_{0.3}(H_2O)_{1.8}$).

composition ratios from TGA. A possible explanation for this observation is due to the solid-phase separations, which was not controllable experimentally, thus affecting the homogeneity of the samples.

3.3. Differential scanning calorimetry (DSC)

DSC provided important information on *thermal transitions* occurring in the nanocomposites. **Figure 3** illustrates the results found for POEGO, V_2O_5POEGO 1:1, V_2O_5POEGO 1:4 fine powder phase, and V_2O_5POEGO 1:4 sticky phase, respectively. The significant transitions observed for these nanocomposites were the glass transition temperature (T_g) and the blending temperature (T_e). Other nanocomposites show similar thermal transitions. A complete list of glass transitions and blending temperatures are summarized in Table 3. The glass transition temperature for POEGO is close to the value of −55.0°C previously reported for POEGO of similar composition (see [19], Table 3, $n = 9$).
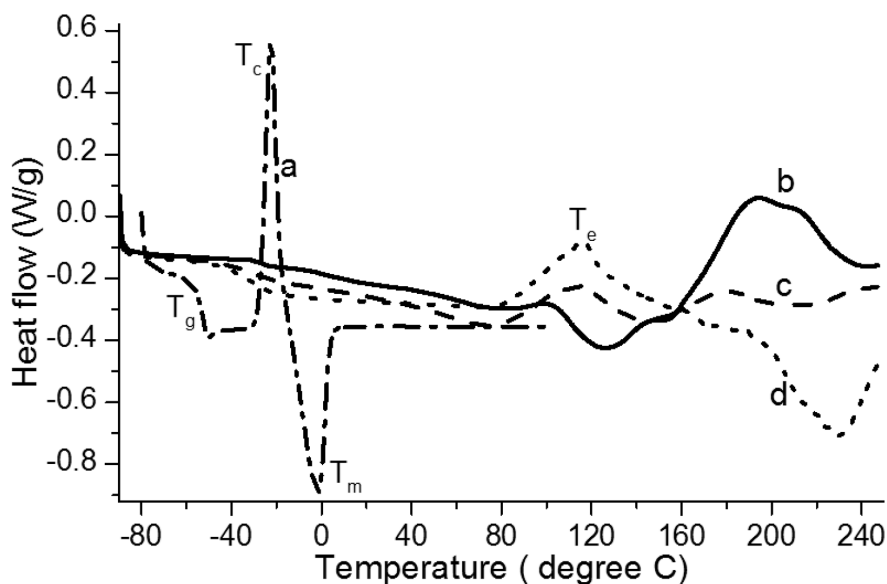

Figure 3. DSC of (a) POEGO, (b) V_2O_5POEGO 1:1, (c) V_2O_5POEGO 1:4 fine powder, and (d) V_2O_5POEGO 1:4 sticky mass at a scan rate of 10°C min^{-1} (T_c is the recrystallization temperature, and T_m is the melting temperature).

Materials (mole ratio)	Phase transitions		ΔT (T_e–T_g)
	T_g (°C)	T_e (°C)	
POEGO	−52.2	–	–
V_2O_5POEGO (1:1)	−25.9	99	124.9
V_2O_5POEGO (1:2)	−25.2	108	133.2
V_2O_5POEGO (1:3) f	−30.4	115	145.4
V_2O_5POEGO (1:3) s	−35.3	113	148.3

Materials (mole ratio)	Phase transitions		ΔT (T_e–T_g)
	T_g (°C)	T_e (°C)	
V_2O_5POEGO (1:4) f	−30.0	115	145.0
V_2O_5POEGO (1:4) s	−31.6	116	147.6

Note. "f" denotes the fine powder phase and "s" denotes the sticky mass phase.

Table 3. DSC thermal transitions for POEGO and nanocomposites.

All samples show negative sloping baselines after the glass transition temperature, which indicates the slow heat flow to the sample, which may correspond to the energy used to vaporize volatiles from the samples during heating. The horizontal baseline displayed by the sticky phase (**Figure 3**, curve d) means that the sample and the reference cell are in thermodynamic equilibrium. This observation is characteristic for amorphous and flexible materials [26].

The blending temperature being below the decomposition temperature (<200°C) means that thin films can be obtained by hot pressing the fine powder or the sticky mass up to 100°C, without any decomposition or damage.

The DSC comparison between POEGO (**Figure 3**, curve a) and V_2O_5POEGO 1:4 sticky mass phase (**Figure 3**, curve d) showed that the sticky mass phase did not have any crystallization or melting *thermal transitions* between the glass transition and the blending temperatures. This observation means that the sticky mass phases are amorphous and flexible between the glass transition and the blending temperatures. This is a significant finding because amorphous polymers are known to be better ionic conductors than their crystalline counterparts. In addition, the stickiness improves the binding ability of the materials, making the nanocomposites good candidates for solid electrolyte and/or cathode materials for lithium/Li-ion batteries.

The temperature gap (ΔT) between T_g and T_e was calculated for each sample and is shown in Table 3. The glass transition temperatures of the nanocomposites are higher than that of pure POEGO (Table 3), because the nanocomposites are more rigid than POEGO, and are hence easily turned into the glassy state.

3.4. Fourier transform infrared (FTIR)

FTIR spectroscopy was used to investigate the type of chemical bonds present in the nanocomposites in comparison to POEGO and pristine V_2O_5nH$_2$O. **Figure 4** shows the IR spectra for POEGO, V_2O_5nH$_2$O, V_2O_5POEGO 1:1, and V_2O_5POEGO 1:4 sticky mass, respectively. IR spectra for all nanocomposites exhibit similar features. The IR band assignments were as follows: POEGO v_{max}/cm^{-1} 2872w, 952 and 861 (CH), 1770s and 1745s

(COCO), and 1115s (C–O–C); $V_2O_5 n H_2O$ ν_{max}/cm^{-1} 1616 (HOH), 999 (V=O), and 707 (V–O–V); and a typical nanocomposite V_2O_5POEGO 1:1 ν_{max}/cm^{-1} 2867 and 941 (CH), 1623 (COCO), 1082, 1021, and 986 (C–O–C and V=O).

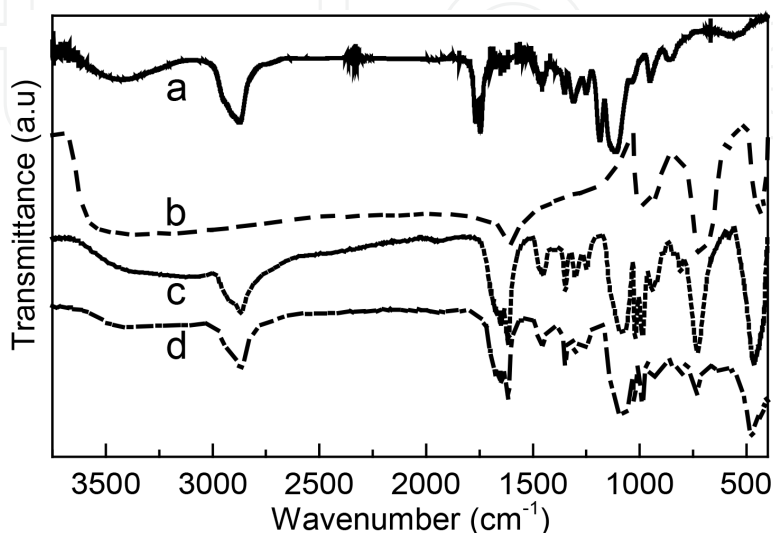**Figure 4** FTIR spectrum for (a) POEGO, (b) $V_2O_5 n H_2O$, (c) V_2O_5POEGO 1:1, and (d) V_2O_5POEGO 1:4 sticky mass.

It is important to note that comparison of the IR spectra for $V_2O_5 n H_2O$ among various literature reports is complicated due to the distinct structural differences associated with the methods of $V_2O_5 n H_2O$ preparation and the aging period of the precursor solutions. In general [27], the characteristic V=O stretching absorption bands are found within the 950–1020 cm^{-1} range, while the bridging V–O–V stretching absorption bands usually occur between 700 and 900 cm^{-1}. The IR bands below 600 cm^{-1} correspond to either edge-sharing V–O stretching or bridging V–O–V deformation vibrations.

The absorption bands for C=O and V=O were significantly perturbed in the nanocomposites, an indication for a chemical reaction between POEGO and $V_2O_5 n H_2O$ during intercalation. However, the presence of bands at 2867, 1082, 986, and 1021 cm^{-1} confirms that the structure of the parent polymer and that of the layered structure are retained to some degree in the nanocomposites. It is not conclusive as to what kind of new chemical bonds are formed. The C–H stretching vibrations for POEGO shifted from 2872 cm^{-1} to between 2867 and 2845 cm^{-1} in the nanocomposites. This band shift provides evidence of an interaction between the polymer and the layered structure.

3.5. AC impedance spectroscopy

The impedance experiment involved applying an AC voltage to the sample and measuring the real and imaginary parts of the resulting current. Curve (a) in **Figure 5** is a complex plane plot of the impedance of a Li-POEGO cast-film sample at a temperature of 310 K. High-

frequency data is near the origin. A semicircle like this, with a low-frequency diagonal spur on the right, is characteristic of an ionic conductor between blocking electrodes [28]. Also shown is a fit to the equivalent-circuit model shown in the inset in **Figure 5**. In this circuit, R is the ionic resistance of the sample, C includes the sample capacitance but is dominated by cable capacitance in parallel with it, and the constant phase element CPE models electrode effects. From the fit, we get $R = (4.43 \pm .04) \times 10^7 \, \Omega$. The sample had a length between electrodes of 9.2 mm, a width of 8.6 mm, and a thickness of $(50 \pm 10) \, \mu m$. The ionic conductivity calculated from R and the sample dimensions is $(5 \pm 1) \times 10^{-6}$ S/cm. This is within the range previously reported for Li-POEGO [19], but is less than the earlier data for Li-POEGO with nine repeat units in the oligomers (see, e.g., [19], **Figure 4**, $n = 9$). The difference may be related to different sample preparation techniques; the earlier measurements were made using dip-type cells, while our samples are cast films.
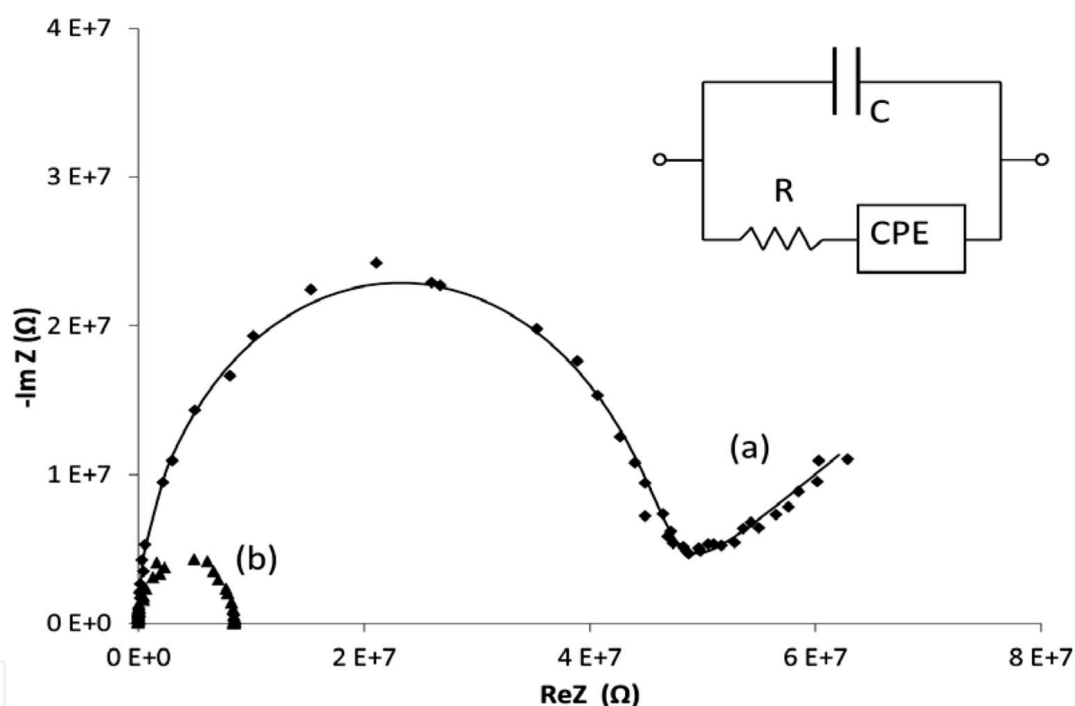

Figure 5 (a) Complex plane plot of the impedance of Li-POEGO at 310 K. The line is a fit to the equivalent circuit shown in the inset. (b) Impedance data for V_2O_5POEGO 1:4 at 300 K.

Impedance data for a typical nanocomposite, V_2O_5POEGO 1:4 (batch EM1-77), at 300 K, is also shown in **Figure 5** (curve b). The plots for all our nanocomposites are semicircles, similar to the plots for a simple parallel RC circuit, indicating that the nanocomposites are electronic conductors. Here, R is the resistance of the sample and C is the total capacitance in parallel with it. C includes the cable capacitance and the capacitance due to the interfaces between the silver paste electrodes and the V_2O_5POEGO sample. We find experimentally that when C is determined by fitting impedance data on these samples, the value of C is equal, within experimental error, to the cable capacitance alone (about 310 pF in our system). This indicates that other contributions to C are very small in comparison. The value of R can be determined

directly from the complex-plane plot, since the low-frequency end of the semicircle terminates on the real axis at R (frequency decreases from left to right). Conductivity (σ) is then calculated from R and the dimensions of the sample. For example, the sample shown in **Figure 5(b)** had $R = (8.52 \pm 0.05) \times 10^6 \, \Omega$, length between electrodes of 6.9 mm, a width of 9.5 mm, and a thickness of $(18 \pm 6) \, \mu m$. The conductivity is therefore $(4.7 \pm 1.6) \times 10^{-5}$ S/cm. The large uncertainty in the thickness reflects the nonuniform thickness of the cast films. This is the main source of uncertainty in all of our conductivity values.

Electronic conductivity data for $V_2O_5nH_2O$ xerogel, and for a number of nanocomposite samples, are shown as a function of inverse temperature in **Figure 6**. The conductivity of $V_2O_5nH_2O$ (3.0×10^{-3} S/cm at 300 K) is comparable to the values reported in the literature. Reported conductivity values for $V_2O_5nH_2O$ vary widely, however, due to many variable experimental parameters, such as the state of vanadium reduction, the relative humidity of the atmosphere, the age of the gel, the sample film dimensions, and the direction of conductivity measurements. All these parameters affect the conductivity of $V_2O_5nH_2O$. For example, due to the layered structure of $V_2O_5nH_2O$, its conductivity can be four orders of magnitude larger when measurements are performed in a direction parallel to the ribbons rather than perpendicular to the ribbons [29]. The conductivities reported in this work were measured approximately parallel to the ribbons, that is, the current flow was along the film, parallel to the substrate.
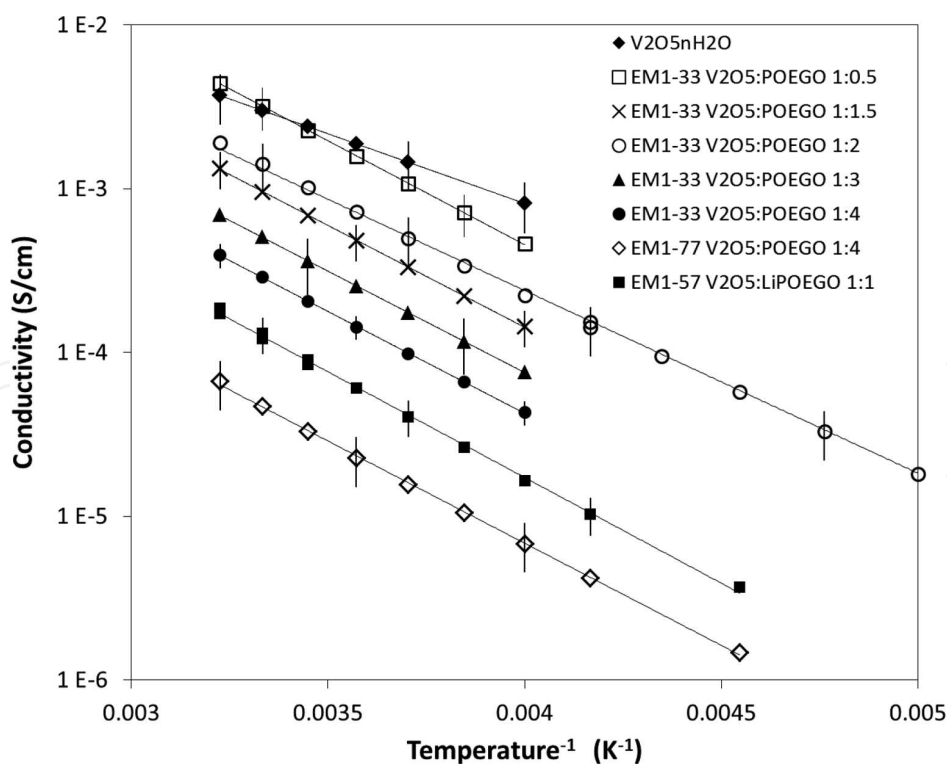

Figure 6 Temperature-dependent conductivities of $V_2O_5nH_2O$, and V_2O_5POEGO nanocomposites. To avoid clutter, error bars are shown only for a few representative points. Uncertainties for other points are similar.

The results for the nanocomposite samples from sample group EM1-33, which were all made at the same time, using the same $V_2O_5nH_2O$ and POEGO starting materials, clearly show the general trend that conductivity decreases as the amount of intercalated POEGO increases. This is consistent with the fact that POEGO is an electrical insulator. Samples made from different batches of starting materials showed a similar trend, but the conductivity values were not consistent from one batch to the next. One example is shown in the **figure 6**: the V_2O_5POEGO 1:4 nanocomposite from batch EM1-77 had a conductivity more than six times lower than that of the V_2O_5POEGO 1:4 nanocomposite from batch EM1-33. This variability between batches is not surprising, given the variability in the conductivity of $V_2O_5nH_2O$ mentioned earlier.

Conductivities of a few V_2O_5LiPOEGO nanocomposites were also measured, and one typical sample is included in **Figure 6**. In general, the electrical conductivity of V_2O_5LiPOEGO was less than that of V_2O_5POEGO. We were not able to detect any signs of ionic conductivity in the V_2O_5LiPOEGO nanocomposites. However, with the impedance technique used in this work, if the ionic conductivity is much smaller than the electronic conductivity, it will not be detected. A material like V_2O_5LiPOEGO 1:4 is expected to conduct lithium ions, and these experiments do not rule that out, since as long as the ionic conductivity is below about 10^{-5} S/cm at 300 K, we would not be able to observe it.

When conductivity data plot as straight lines in an Arrhenius-type plot like **Figure 6**, this indicates a thermally activated conduction process described by an equation of the form

$$\sigma(T) = \sigma_0 e^{-E/kT}$$

where σ_0 is a constant and E is the activation energy (or semiconductor band gap). Fits to this equation are shown as solid lines in **Figure 6**, and the activation energies were found from the slopes of these lines. For $V_2O_5nH_2O$, we get $E = 0.17$ eV, close to the values reported in the literature [29, 30]. All the nanocomposites have activation energies in the range 0.23–0.26 eV, very close to each other and significantly higher than that for $V_2O_5nH_2O$. This can be seen directly in the graph where the nanocomposite lines all have roughly the same slope, and all have a steeper slope than $V_2O_5nH_2O$. We conclude that insertion of PEOGO into vanadium pentoxide increases the band gap. A similar effect was seen when poly(oxymethylene-oxyethylene) (POMOE) was inserted into $V_2O_5nH_2O$ [31].

Note that the band gap does not depend on the V_2O_5:POEGO ratio. Our XRD data shows that interlayer expansion is also almost independent of V_2O_5:POEGO ratio, indicating that the interlayer spaces are fully occupied with a bilayer arrangement of POEGO chains even before the ratio reaches 1:1. Since increasing the amount of POEGO further does not result in more POEGO between the V_2O_5 layers, some of the POEGO must be outside the nanocomposite crystallites. This interpretation of the XRD data explains two features of the conductivity. First, assuming the increase in activation energy is due to separation of the V_2O_5 layers and/or interaction between the V_2O_5 layers and the inserted polymers, there should be no further change in activation energy once the interlayer spaces are full. Second, as the amount of POEGO is increased beyond what is needed to fill the interlayer spaces, regions of electrically

insulating polymer will form outside the nanocomposite crystallites, blocking some charge-transport channels and reducing the conductivity through the sample.

Since the conductivity measurements were made with cast films in which phase separation does not occur, we have not yet acquired the conductivity data on the separate fine powder and sticky mass phases obtained from freeze-dried V_2O_5POEGO 1:3 and V_2O_5POEGO 1:4. Characterization of charge transport in these phases would be an interesting topic for future work. Because of the high polymer content in the sticky mass phase, complexing it with a lithium salt may yield a material with higher ionic conductivity.

4. Conclusions

In summary, successful intercalation of POEGO and Li-POEGO into $V_2O_5nH_2O$ at room temperature is demonstrated. The sticky mass phases of the nanocomposites obtained upon freeze-drying the mole ratios above 1:3 have appealing properties, as they are thermally stable in air up to around 200°C and amorphous in the temperature range (−30°C to 100°C). The cast film nanocomposites we studied using AC impedance spectroscopy are not suitable for solid electrolyte applications because of their electronic conductivity. $V_2O_5LiPOEGO$ nanocomposites prepared using cast film methods are believed to be conductors of both electrons and lithium ions, and therefore may have applications as electrode materials in Li-ion batteries. The next challenge is to further characterize the phase-separated materials produced by freeze-drying.

Acknowledgements

Author details

Evans A. Monyoncho[1], Rabin Bissessur[1*], Douglas C. Dahn[2] and Victoria Trenton[2]

*Address all correspondence to: rabissessur@upei.ca

1 Chemistry Department, University of Prince Edward Island, Charlottetown, PE, Canada

2 Physics Department, University of Prince Edward Island, Charlottetown, PE, Canada

References

[1]   Yang Z, Zhang J, Kintner-Meyer MCW, Lu X, Choi D, Lemmon JP, Liu J. Electrochemical energy storage for green grid. *Chem Rev* 2011;111:3577–3613.

[2]   Baddour R, Pereira-Ramos JP, Messina R, Perichon J. Vanadium pentoxide xerogel as rechargeable cathodic material for lithium batteries. *J Electroanal Chem* 1990;277:359–366.

[3]   Tsiafoulis CG, Florou AB, Trikalitis PN, Bakas T, Prodromidis MI. Electrochemical study of ferrocene intercalated vanadium pentoxide xerogel/polyvinyl alcohol composite films: application in the development of amperometric biosensors. *Electrochem Commun* 2005;7:781–88.

[4]   Toma HE. Vanadium(V) oxide—metal organic nanocomposites as electrochemical sensing materials. *Mater Sci Forum* 2010;636:729.

[5]   Müller-Warmuth W, Schöllhorn R. *Progress in Intercalation Research*. In *Physics and Chemistry of Materials with Low-dimension Structures*. Kluwer Academic Publishers, USA, 1994, Vol. 17, pp. 536.

[6]   Pomogailo AD. Synthesis and intercalation chemistry of hybrid organic and inorganic nanocomposites. *Polym Sci* 2006;48:85–111.

[7]   Zakharova GS, Volkov VL. Intercalation compounds based on vanadium(V) oxide xerogel. *Russ Chem Rev* 2003;72:311–325.

[8]   Wu CG, Kanatzidis MG. Layered vanadium pentoxide xerogels: host-guest chemistry and conductive-polymers. *Mater Res Soc Symp Proc* 1991;210:429–442.

[9]   Passerini S, Chang D, Chu X, Ba Le D, Smyrl W. Spin-coated V_2O_5 xerogel thin films. 1. Microstructure and morphology. *Chem Mater* 1995;7:780–85.

[10] Ramzy A, Thangadurai V. Tailor-made development of fast Li Ion conducting garnet-like solid electrolytes. *ACS Appl Mater Interfaces* 2010;2:385–390.

[11] Dietrich Berndt. *Batteries*, 3. Secondary Batteries. In *Ullmann's Encyclopedia of Industrial Chemistry*. Wiley-VCH Verlag GmbH & Co. KGaA, 2014, 1–68.

[12] Fenton DE, Parker JM, Wright PV. Complexes of alkali metal ions with poly(ethylene oxide). *Polymer* 1973;14:589.

[13] Wright PV. Electrical conductivity in ionic complexes of poly(ethylene oxide). *Br Polym J* 1975;7:319–327.

[14] Armand MB, Chabagno JM, Duclot M. In *Poly-ethers as solid electrolytes*. Vashitshta P, Mundy JN, Shenoy GK, editors, Second International Meeting on Solid Electrolytes, North Holland Publishers, 1978. Amsterdam, Netherlands.

[15] Quartarone E, Mustarelli P, Magistris A. PEO-based composite polymer electrolytes. *Solid State Ionics* 1998;110:1–14.

[16] MacCallum JR. In *Polymer Electrolyte Reviews*, MacCallum JR and Vincent CA, editors, Elsevier Applied Science, 1987. London and New York.

[17] Forsyth M, Tipton AL, Shriver DF, Ratner MA, Mac Farlane DR. Ionic conductivity in poly(diethylene glycol-carbonate)/sodium triflate complexes. *Solid State Ionics* 1997;99:257–261.

[18] Xu K, Zhou T, Deng ZH, WanGX. *Chin J Polym Sci* 1992;10:223.

[19] Xu W, Belieres J, Angell A. Ionic conductivity and electrochemical stability of poly[oligo(ethylene glycol)oxalate]-lithium salt complexes. *Chem Mater* 2001;13:575–380.

[20] Scully SF, Bissessur R. Encapsulation of polymer electrolytes into hectorite. *Appl Clay Sci* 2010; 47:444–447.

[21] Bissessur R, Schipper D. Exfoliation and reconstruction of Sn S_2 layers: a synthetic route for the preparation of polymer-Sn S_2 nanomaterials. *Mater Lett* 2008;62:1638–1641.

[22] Bissessur R, ScullySF. Intercalation of solid polymer electrolytes into graphite oxide. *Solid State Ionics* 2007;178:877–882.

[23] Bissessur R, Gallant D, Brüning R. Novel Intercalation compound of poly[oligo(ethylene glycol)-oxalate in molybdenum disulfide. *J Mater Sci Lett* 2003;22:429–431.

[24] Guerra EM, Ciuffi KJ, Oliveira HP. V_2O_5 xerogel–poly(ethylene oxide) hybrid material: synthesis, characterization, and electrochemical properties. *J Solid State Chem* 2006;179:3814–3823.

[25] Livage J. Synthesis of polyoxovanadates via "chimie douce". *Coord Chem Rev* 1998:178/180:999–1018.

[26] Wunderlich B. *Thermal Analysis of Polymeric Materials*. Springer-Verlag, Berlin; Heidelberg, Berlin, Heidelberg, 2005.

[27] Anaissi FJ, Demets GJ, Alvarez EB, Politi MJ, Toma H.E. Long-term aging of vanadium(V) oxide xerogel precursor solutions: structural and electrochemical implications. *Electrochim Acta* 2001;47:441–450.

[28] Barsoukov E. In Macdonald JR, editors. *Impedance Spectroscopy*: *Theory*, *Experiment*, *and Applications*. John Wiley & Sons, Hoboken, New Jersey, USA, 2005.

[29] Livage J. Vanadium pentoxide gels. *Chem Mater* 1991;3:578–593.

[30] De S, Dey A, De SK. Characterization and transport properties of intercalated polypyrrole- vanadium pentoxide xerogel nanocomposite. *Solid State Commun* 2006;137:662–667.

[31] Monyoncho E, Bissessur R, Trenton V, Dahn DC. A bilayer insertion of poly(oxy-methylene-oxyethylene) into vanadium oxide xerogel: preparation, characterization and insertion mechanism. *Solid State Ionics* 2012;227:1–9.